PROCEEDINGS OF SCIENCE

ICRC 2021
THE ASTROPARTICLE PHYSICS CONFERENCE
Berlin | Germany
37th International Cosmic Ray Conference
12–23 July 2021

A Decade of the Askaryan Radio Array

Kara Hoffman[a,*] **on behalf of the ARA Collaboration**
(a complete list of authors can be found at the end of the proceedings)

[a] *University of Maryland,*
College Park, MD
E-mail: kara@umd.edu

The Askaryan Radio Array has developed the hardware and analysis techniques required to realize an observatory scale array for the detection of ultra high energy neutrinos in the radio frequency detection channel, while also delivering world competitive limits on the high energy neutrino flux. The first ARA instrumentation was installed in the Antarctic ice cap near the geographic South Pole over a decade ago. The addition of each new cluster of antennas in the ice brought improvement and innovation. The final installation in the austral summer of 2017-2018 included a "phased array" trigger which demonstrated the ability to increase the trigger efficiency using interferometric information in real time. ARA's detailed in situ measurements of the propagation of radio frequency signals in the ice have established the polar ice cap as an ideal host for such an array, while informing the reconstruction and simulation of in ice events. With five deep radio antenna clusters are currently operating at the South Pole, current ARA results boast world competitive sensitivity to ultra high energy neutrinos, while the data currently on disk holds the promise of extending these results to lower fluxes in the near future. Following on the success of ARA, two new embedded in ice arrays have been planned, RNO-G and IceCube Gen2.

37th International Cosmic Ray Conference (ICRC 2021)
July 12th – 23rd, 2021
Online – Berlin, Germany

*Presenter

PoS(ICRC2021)014

1. Introduction

Neutrinos are in many ways the ideal astronomical messenger. Their lack of charge and tiny mass allows them to reach us from dense and distant corners of the universe, shedding light on the enigma of cosmic rays, and providing insights into the structure of some of the cosmos' most energetic objects. However, the very lack of reactivity that makes them such powerful messengers also makes them difficult to detect, requiring the instrumentation of large target volumes to be sensitive to the small flux at high energies. Radio frequency emission from neutrino induced particle showers in dense media was proposed by Askaryan [1] as a detection mechanism for ultra high energy interactions, allowing the monitoring of vast areas with relatively sparse instrumentation. This approach is particularly well suited to the search for a "cosmogenic" population [2] of ultra high energy neutrinos expected from the interaction of cosmic rays on the cosmic microwave background with energies above the pion photoproduction threshold. In the past two decades, several pioneering efforts have developed the technique. Some have taken a synoptic view, monitoring the target medium from a distance, such as NuMoon's observations of the lunar regolith from ground based radio telescopes [3], while others employed embedded antennas, a tactic taken by RICE [4] to monitor the Antarctic ice.

The Askaryan Radio Array (ARA) was conceived to further develop the embedded technique in the pristine ice near the geographic South Pole, and served as a springboard to develop the simulation, analysis techniques, and instrumentation necessary to realize an observatory scale array. At the same time, the scale of the array was chosen to provide world leading sensitivity to neutrinos in the energy range from 10^8 – 10^{10} GeV. Since it's inception, the discovery of a diffuse flux of astrophysical neutrinos [5] by the IceCube Collaboration and the identification of the first candidate neutrino source [6] provided the motivation to push the energy threshold of the technology downward with the goal of extending the measurement of the detected astrophysical flux to higher energies. This has been successfully demonstrated with the development and installation of the phased array.

This proceeding will give an overview the design, development, and science results of ARA since the first test instrumentation was installed in the austral summer of 2010-2011, as well as its future sensitivity.

2. The ARA Instrument

ARA is composed of five clusters of antennas embedded in the clear, deep ice near the Amundsen Scott South Pole Station. Each cluster is installed in 6 narrow boreholes, up to 200 m in depth as shown in Figure 1. Four of these contain receiver antennas, with two horizontally polarized (Hpol) and two vertically polarized (Vpol) antennas in each hole. The remaining two boreholes each house a calibration device which can generate either a narrow pulse or a flat noise spectrum at various levels of attenuation broadcast through either an attached Vpol or Hpol antenna. Each set of receiving antennas (Vpol and Hpol) are installed at the corner of a cube measuring $\sim$ 20 m on a side. The newest station, labeled A5 in Figure 1, contains one additional densely instrumented string in its center, as described below in Section 6. The stations are spaced 2 kms apart. The array is optimized for 100-850 MHz band.

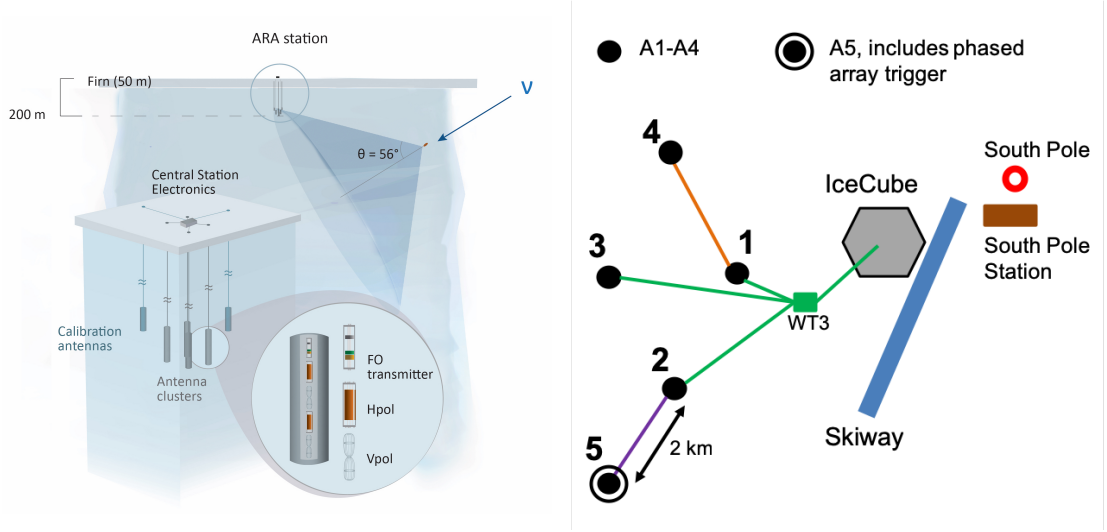

Figure 1: The geometry of the ARA array. **Left:** A schematic of an ARA station showing the orientation of the antennas (far left), the arrangement of the antennas within a borehole (bottom inset), and the sampling of a Cerenkov cone (top). **Right:** The footprint of the array and its orientation with respect to IceCube and the South Pole Station.

The spacing and the geometry of the clusters allows each station to operate autonomously, while completely reconstructing the Cerenkov cone using timing and polarization information. A trigger is formed when the power in three of the eight antennas of the same polarization exceed 5 times the noise rate in a time profile that is consistent with an electromagnetic wave traversing the array. The trigger threshold is dynamically adjusted to fix the trigger rate at 5 Hz. Because the electric field of the Askaryan radiation is oriented normal to the surface of the Cerenkov cone, the polarization information can be used to determine the direction and orientation of the cone. Due to the gradual compaction of snow into ice, the shallow layers, labelled as "firn" in the left panel of Figure 1, exhibit a varying index of refraction, resulting in a mirroring effect near the surface. This gives rise to dual direct and reflected/refracted ray paths, which provide a constraint on the distance to the event vertex.

3. Ice Properties

Over the course of the operation of ARA, a number of different devices have been used to study the properties of the ice. In the austral summer preceding the installation of the first ARA station, a shallow "TestBed" of large, broadband antennas was installed as a platform to study antenna prototypes, as well as to study the noise profile of the ARA site. In addition, three high voltage ($\approx$ 5 kV) radio pulse generators were installed parasitically on IceCube strings during their last deployment season at depths of 2450m and 1450m. These devices provided the first in situ probe of point to point propagation of radio waves in the deep ice. The signal absorption varies as a function of depth as a result of a temperature gradient, owing to the geothermal warming near the bedrock, but the attenuation length was found to be 1.45 ± 0.25 km in the top 1500 m of ice [7]. This measurement validated ARA's planned approach of monitoring large swaths of ice for high energy

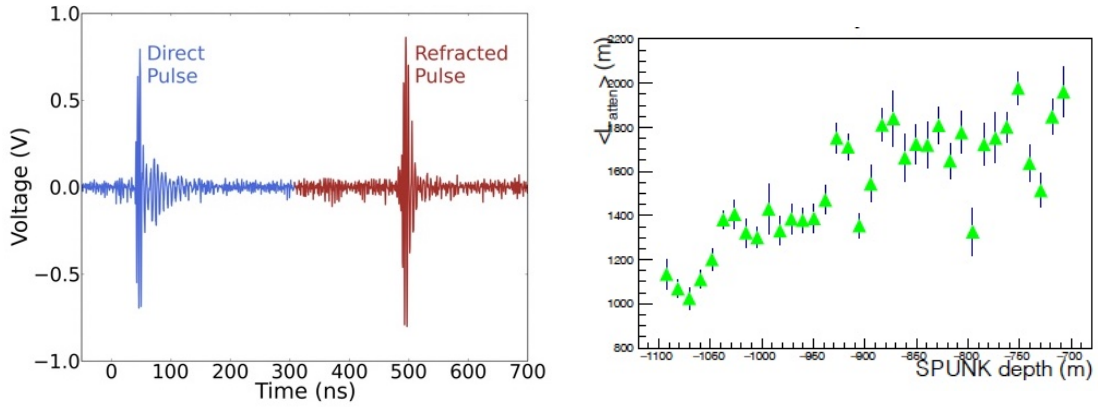

Figure 2: Left: The two separate pulses arriving from the same event during the retrievable pulser runs: the "direct" pulse, and the "refracted" pulse, which is reflected from the firn layer of the shallow ice. **Right:** The measured attenaution length as a function of depth obtained from a run of the retrievable pulse generator.

particle showers with sparse instrumentation. In addition, the noise power density was found to be excellent over the sensitive band of the instrument.

Since the installation of the deep ARA stations, additional studies of the RF transmission through the ice have been performed using a retrievable pulse generator mounted on a winch and lowered into a 1700m deep hole, created by the South Pole Ice Core Project, that is located between 1257m (Station 1) and 4164m (Station5) from the ARA stations. This allowed a careful study of the signal propagation over multiple baselines as a function of depth. [8] These studies yielded several consequential results. First, it confirmed the long attenuation length measured from the deep pulse generator. Second, careful studies of the time lag between the "direct" ray from the source and the "refracted" ray mirrored from the surface, an example of which is shown in Figure 2, allows the range to the source vertex to be determine to $\approx$ 15 %, which will prove to be a powerful tool in the event reconstruction. In addition, the index of refraction as a function of depth was measured and the "shadow" zone, or the region inaccessible to due ray tracing effects, was carefully mapped out. Finally, asymmetries in the propagation of the horizontal vs. vertical polarizations (known as "birefrigence") was measured to the 0.15 % level. All of these finding indicate that the ice near the South Pole is a ideal platform for ARA and future Askaryan detectors.

4. Event Reconstruction

The ability to reconstruct the direction of a signal in the ice is critical for both background suppression of surface anthropegenic noise, as well as in identifying astrophysical point sources. The cubic arrangement of the antennas within a station allow the traverse time of any signal to be measured over multiple baselines to obtain a true direction. For each pair of antennas, the process starts by calculating the cross correlation function

$$C_{i,j} = \frac{\sum_t V_i(t) V_j(t+\tau)}{RMS_i \times RMS_j} \tag{1}$$

which is maximized for the true time lag τ between two antennas recording voltages as a function of time of V_i and V_j respectively. Each pair of antennas defines a ring of probability along the axis

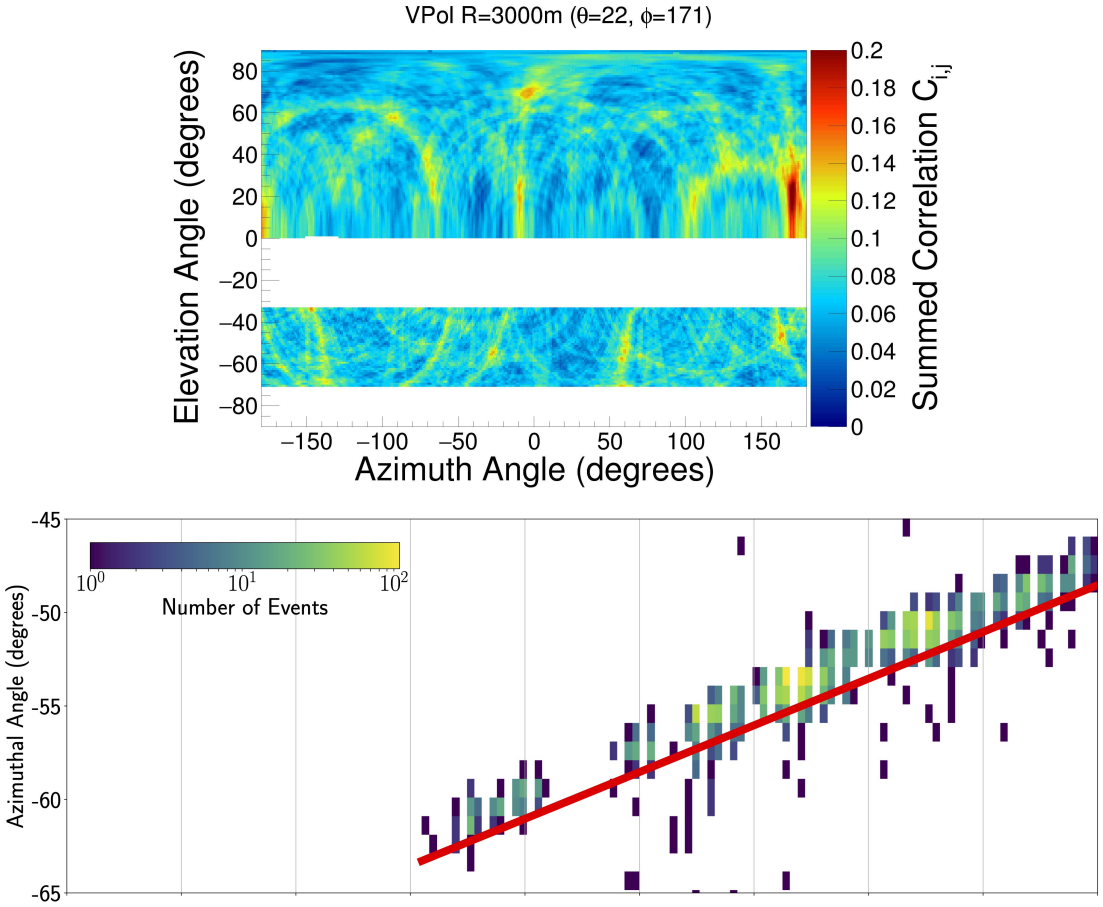

Figure 3: Top: The reconstructed interferometric map of an event trigger occurring during the February 15, 2011 solar flare. The blank strips are the location of areas inaccessible due to ray tracing (middle) and the bedrock (bottom). **Bottom:** The reconstructed azimuth of the events associated with the solar flare, compared with the known location of the sun (red line). The reconstructed direction tracks the location of the sun in azimuth with a 2 degree offset.

connecting the two antennas. The most probable direction of the incoming signal is determined by the intersection of the rings of probability determined by each of the antenna pairs on an interferometric map.

On February 15, 2011, an excess of ≈ 2000 radio emission events were observed in the newly installed ARA TestBed over a period of 70 minutes [9]. The period during which the events were observed was coincident with a known solar flare, and a subsequent analysis of the events show that the direction of the reconstructed events tracks the position of the sun on the sky with a 2 degree systematic offset in azimuth and a 10 degree systematic offset in zenith. Figure 3 shows an interferometric map reconstruction of one of the events at the top, and the reconstructed azimuth of all of the events shown on the bottom, with the known location of the sun shown as a red line. Although the array was designed to detect englacial events, with signals emanating from nearby points in the ice, this event served as a fortuitous confirmation of ARA's reconstruction capabilities and a unique opportunity to study a potential natural source of radio frequency background. In

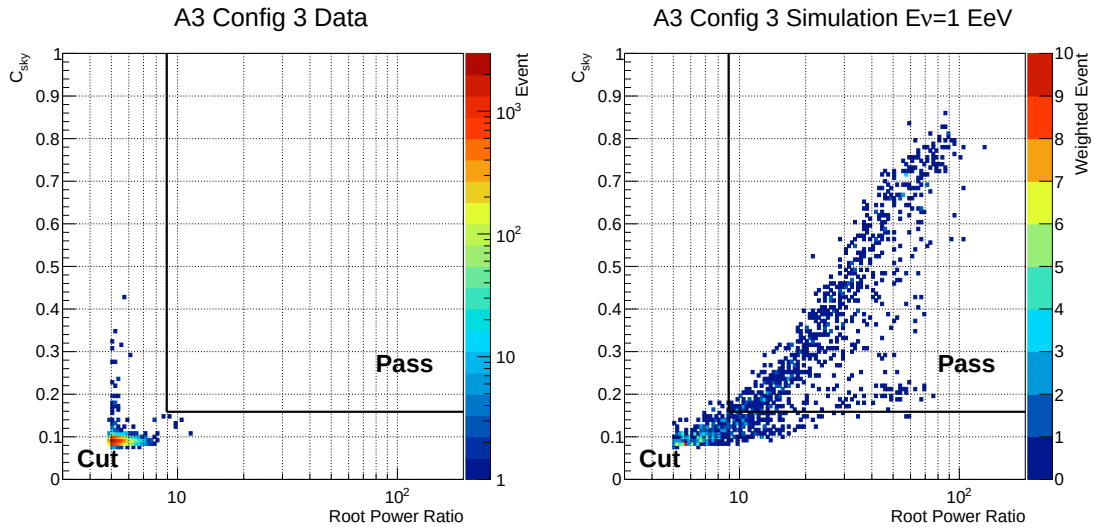

Figure 4: The bivariate cut plane is shown for ARA station 3. **Left:** The chosen cut is shown for the 10% burn sample to eliminate some low-correlation, low power events. **Right:** However, the cut is efficient for simulated 10^{18} eV neutrinos.

addition, it opens the possibility of radio astrophysics observations by ARA, given its broad field of view and bandwidth.

5. ARA Neutrino Searches

ARA was primarily designed to detect radio frequency signal emissions from ultra high energy neutrino interactions in the ice and, to date, ARA has published the result of a number of such searches [10, 11], establishing the array as a leading instrument in this energy regime. Most recently, a search for a diffuse flux neutrinos using 2 stations (labeled A2 and A3 in Figure 1) and 1000 days of data has been published [12]. Two independent analyses were developed for this search, yielding similar results. Both analyses were blind to avoid bias and used 10% of the data to tune the event selection criteria before examining the entire sample. Noise was separated from neutrino signal using a simple bivariate cut in the plane of the peak cross correlation, C_{sky}, vs. signal strength, Γ. This can be seen in Figure 4 for station 3 to provide good separation between noise and expected neutrino signals. Both analyses find 0 events on a background expectation of $(5 \pm 2) \times 10^{-2}$ for the first analysis, and $(1.0 \pm 0.3) \times 10^{-2}$ for the other. This analysis places an all flavor upper limit of $EF(E) = 5.6 \times 10^{-16} \mathrm{cm}^{-2}\mathrm{s}^{-1}\mathrm{sr}^{-1}$ at an energy of 10^{18} eV.

6. The Phased Array

Distinguishing radio frequency signal originating from distant particle showers in the ice from random coincident thermal noise events with good efficiency poses a challenge in designing any array. The approach implemented in the ARA global trigger of requiring multiple antennas to trigger within a causal time window limits the sensitivity to events that are at least 3-4 times the thermal noise level. Further, for an embedded array, the gain of the antennas used is limited by

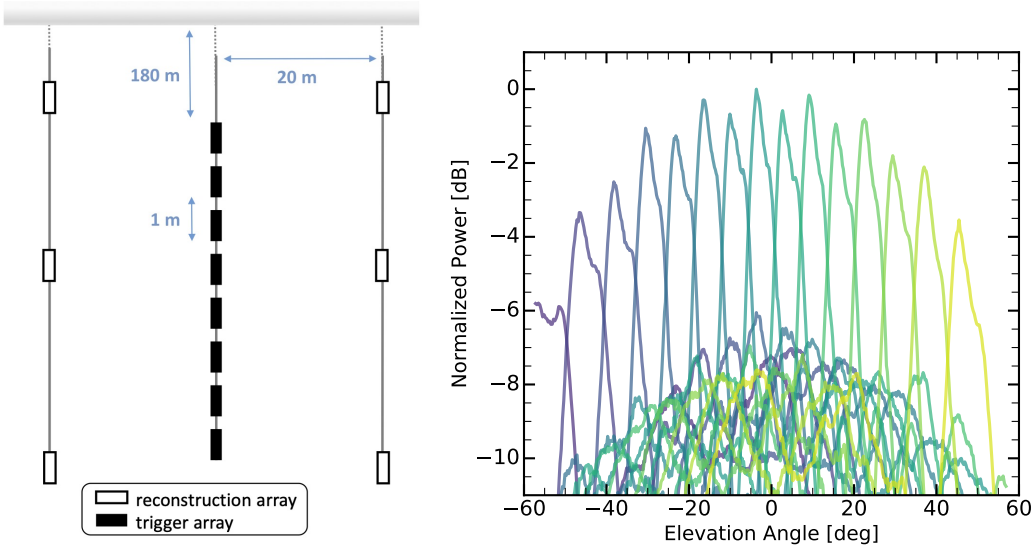

Figure 5: Left: A schematic of the phased array, which consists of a densely instrumented string of vertically polarized antennas installed in a dedicated hole at the center of ARA station 5. **Right:** By measuring time lags of the peak voltages between different antennas, incoming pulses can be compared to the signal expectation for 15 incoming plane wave directions, with the relative power in each beam as a function of elevation angle is shown.

the geometry of the boreholes, about 15 cm for ARA. The trigger efficiency can be improved using interferometry to sum the signals from multiple lower gain antennas in real time as proposed in [13]. Such a "phased array" trigger was implemented in the final ARA station, which was installed in the austral summer of 2017-2018 [14].

A schematic of ARA Station 5 is shown on the left in Figure 5. Station 5 includes a densely instrumented string hosting 7 ARA-style Vpol antennas and 2 Hpol antennas spaced 1-2 m apart with a dedicated trigger, allowing this string to trigger independently from the rest of the station. In every other way, Station 5 shares the same geometry as Stations 1-4. The Phased Array trigger then compares the delays in the incoming signals that expected from a signal from each of 14 predetermined directions given by:

$$\sin(\theta_m) = \frac{cm\Delta t}{nd} \tag{2}$$

where c is the speed of light, m is an integer, Δt is the sampling interval, d is the antenna spacing, and n is the index of refraction of the medium. These directions, or "beams" are shown on the right in Figure 5. The amplitude of a signal will scale with the number of antennas, N, in the correct beam direction, while the amplitude of uncorrelated thermal noise scales as $\sqrt{N}$, allowing the station to trigger at much lower signal to noise ratios (SNRs).

The ARA station 5 phased array has been demonstrated in [14] to become fully efficient at an SNR between 1 and 2, compared to the conventional ARA trigger which turned on at SNRs between 3 and 4. Until now, however, it was unknown whether the gain in signal efficiency would translate into greater efficiency at analysis level, or if the events recovered would be of a quality too poor to reconstruct. During this conference, the results of a first analysis of phased array data using

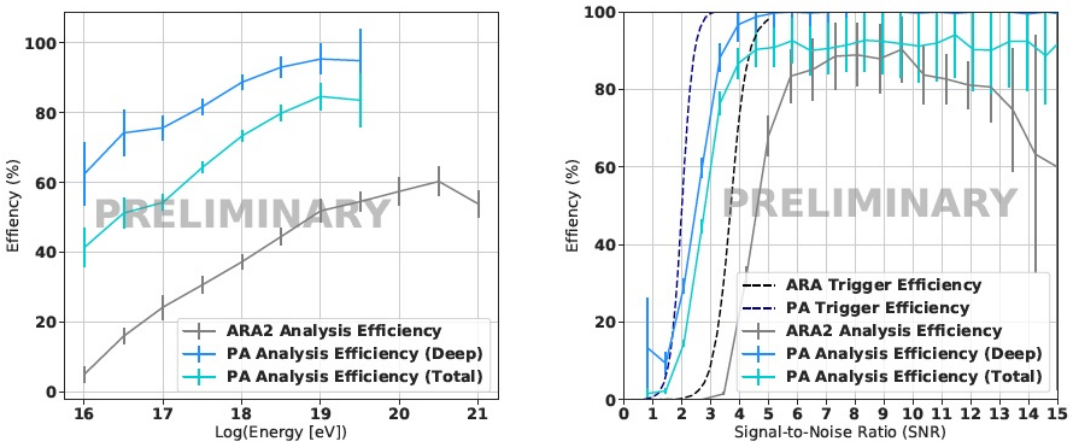

Figure 6: Right: The efficiency at analysis level as a function of energy for the phased array is shown in blue for events in the deep ice, and in cyan when shallow events are included. **Left:** The efficiency as a function of signal to noise ratio for that phased array analysis. For comparison, the efficiency for the two station ARA analysis is also plotted.

208 days of livetime were reported [15]. The analysis divides the data into two interaction regions in the ice, a deep region, which contains 90% of the expected signal, and a shallow region, with a relatively high background rate from anthropogenic activity and impinging cosmic ray air shower cores. Tuning the event selection on a 10% "burn" sample, events failing quality criteria were removed, and a Fisher discriminant was used to separate signal from background. The efficiency of the event selection is shown in Figure 6. In the left panel, the efficiency is shown as a function of neutrino energy for both the deep and surface regions, as well as for the analysis described in Section 5. At the lowest energies, the efficiency is increased by a factor of 10. The right panel displays the efficiency as a function of SNR of the phased array compared to ARA stations 2 and 3 at both trigger level and analysis level. The phased array deep analysis has been unblinded, with one event observed on an expected background of $0.09^{+0.069}_{-0.0316}$. This observed event does not appear to be a thermal noise event and is under investigation. This analysis only uses information from the phased array, however, the trigger conditions were also met for the conventional strings on the host ARA station.

Events reconstructed with the phased array can be reconstructed with excellent precision in elevation and range however, given its azimuthal symmetry, information from the remaining ARA strings are required for azimuthal reconstruction. Recent precision calibrations of antenna positions [16] allow reconstruction using full waveforms, and subdegree angular resolution is obtained.

7. Neutrino Results and Current Sensitivity

A summary of the neutrino flux limits derived from the analyses presented in this proceeding are shown in Figure 7. The limit calculated from the conventional 2 station analysis is shown by the solid black line, while the limit from the deep phased array anlysis is shown by the solid purple line.

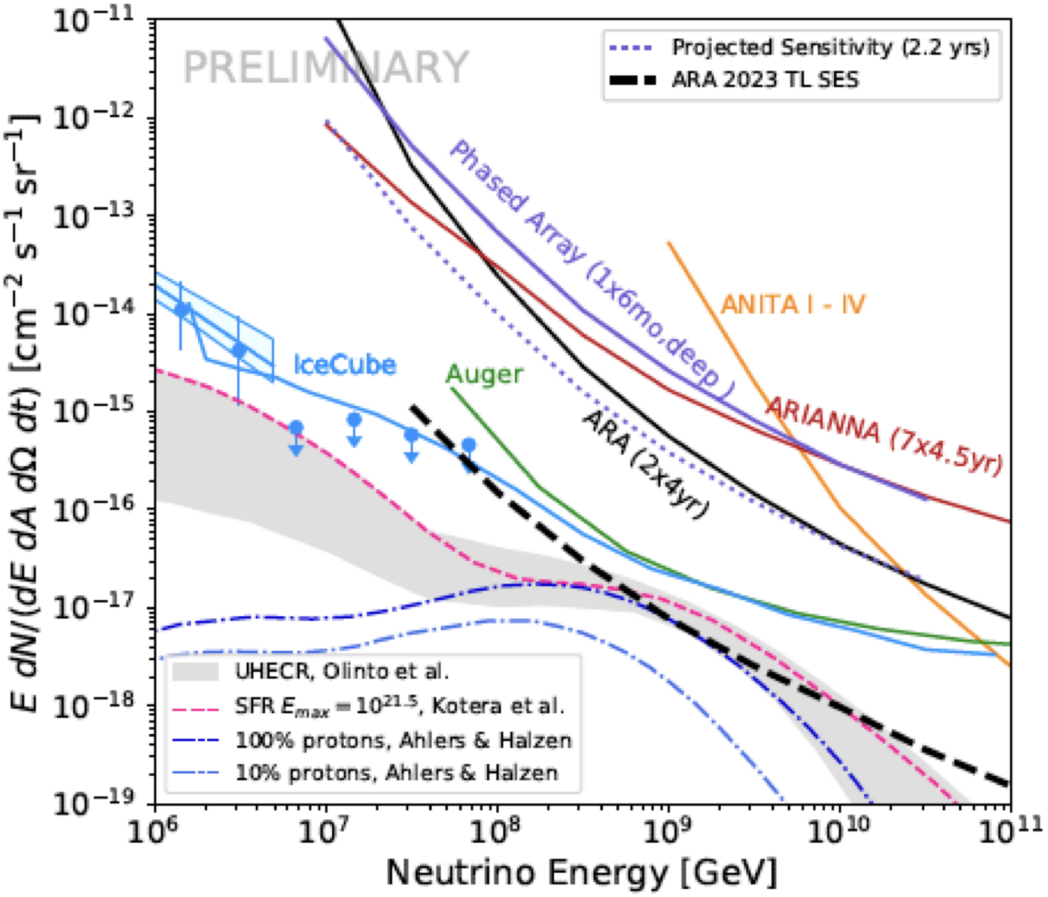

Figure 7: A summary of the ultra high energy neutrino flux limits from currently operating observatories including those derived from the ARA 4 year, 2 station analysis (solid black line), and the six month phased array analysis (solid purple line). Also shown in the porjected sensitivity of the phased array using the data currently on disk (purple dotted line) and the projected single event sensitivity of all ARA data (at trigger level) to be collected through the end of 2023 is shown by the dashed black line.

The results from the phased array comprise less than a quarter of the phased array data currently on disk, and the projected sensitivity of the for the entire phased array dataset collected to date is shown by the purple dotted line. ARA's results are competitive with the other currently operating ultra high energy neutrino arrays, which are also plotted. The projected single event sensitivity at trigger level of the entirety of ARA data projected to be collected through the end of 2023 is illustrated by the black dashed line. This sensitivity begins to meet the flux expectations for cosmogenic neutrinos under favorable assumptions.

Following on the success of ARA, two new in-ice neutrino arrays are planned. ARA has shown the pristine, cold ice near the geographic South Pole to be an ideal medium for the detection of Askaryan radiation. In addition, ARA has demonstrated the hardware and analysis techniques to gain sensitivity to the highest energy neutrinos. IceCube is planning an extensive expansion and upgrade which includes a significant radio component in order to extend the measured flux of

neutrinos several decades in energy [17, 18]. In the meantime, construction is already underway on a northern hemisphere array in Greenland [19]. ARA continues to operate and collect data, and remains a world competitive detector of high energy neutrinos.

References

[1] G. A. Askar'yan. Coherent Radio Emission from Cosmic Showers in Air and in Dense Media. *Soviet Journal of Experimental and Theoretical Physics*, 21:658, September 1965.

[2] V. S. Berezinsky and G. T. Zatsepin. . *Sov. J. Nucl. Phys.*, 11:111, 1970.

[3] O. Scholten, S. Buitink, J. Bacelar, R. Braun, A. G. de Bruyn, H. Falcke, K. Singh, B. Stappers, R. G. Strom, and R. al Yahyaoui. Status report of the numoon experiment, 2008.

[4] I. Kravchenko et al. Rice limits on the diffuse ultrahigh energy neutrino flux. *Phys. Rev.*, D73:082002, 2006.

[5] M. G. Aartsen et al. Observation of High-Energy Astrophysical Neutrinos in Three Years of IceCube Data. *Phys. Rev. Lett.*, 113:101101, 2014.

[6] M. G. Aartsen et al. Multimessenger observations of a flaring blazar coincident with high-energy neutrino IceCube-170922A. *Science*, 361(6398):eaat1378, 2018.

[7] P. Allison, J. Auffenberg, R. Bard, J.J. Beatty, D.Z. Besson, et al. Design and Initial Performance of the Askaryan Radio Array Prototype EeV Neutrino Detector at the South Pole. *Astropart.Phys.*, 35:457–477, 2012.

[8] P. Allison et al. Long-baseline horizontal radio-frequency transmission through polar ice. *Journal of Cosmology and Astroparticle Physics*, 2020(12):009–009, dec 2020.

[9] P. Allison et al. Observation of Reconstructable Radio Emission Coincident with an X-Class Solar Flare in the Askaryan Radio Array Prototype Station. *ArXiv e-prints (Submitted to Astroparticle Physics)*, 2018. arXiv:1807.03335.

[10] P. Allison et al. First Constraints on the Ultra-High Energy Neutrino Flux from a Prototype Station of the Askaryan Radio Array. *Astropart. Phys.*, 70:62–80, 2015.

[11] P. Allison, et al., and ARA Collaboration. Performance of two Askaryan Radio Array stations and first results in the search for ultrahigh energy neutrinos. *Physical Review D*, 93(8):082003, April 2016.

[12] P. Allison et al. Constraints on the diffuse flux of ultrahigh energy neutrinos from four years of Askaryan Radio Array data in two stations. *Phys. Rev. D*, 102(4):043021, 2020.

[13] A. G. Vieregg, K. Bechtol, and A. Romero-Wolf. A Technique for Detection of PeV Neutrinos Using a Phased Radio Array. *JCAP*, 1602(02):005, 2016.

[14] P. Allison et al. Design and performance of an interferometric trigger array for radio detection of high-energy neutrinos. *Nuclear Instruments and Methods in Physics Research Section A: Accelerators, Spectrometers, Detectors and Associated Equipment*, 930:112–125, Jun 2019.

[15] Kaeli Hughes. Implementing a low-threshold analysis with the askaryan radio array (ara). *these proceedings*, 2021.

[16] Paramita Dasgupta and Kaeli Hughes. The calibration of the geometry and antenna delay in askaryan radio array station 4 and 5. *these proceedings*, 2021.

[17] M G Aartsen et al. Icecube-gen2: the window to the extreme universe. *Journal of Physics G: Nuclear and Particle Physics*, 48(6):060501, Apr 2021.

[18] Marek Kowalski. Icecube-gen2: The window to the extreme universe. *these proceedings*, 2021.

[19] Stephanie Wissel. The radio neutrino observatory in greenland (rno-g). *these proceedings*, 2021.

Full Authors List: ARA Collaboration

P. Allison[15], S. Archambault[17], J.J. Beatty [15], M, Beheler-Amass[4], D.Z. Besson [10,13], M. Beydler[4], C.H. Chen [2], P. Chen [2], Y.C. Chen[2], B.A. Clark [16], W. Clay [8], A. Connolly[15], L. Cremonesi [6], P. Dasgupta [18], J. Davies [6], S, De Kockere [9], K.D. de Vries [9], C. Deaconu[8], M, A DuVernois[4], J. Flaherty[15], E. Friedman[3], R. Gaior[17], J. C. Hanson[19], K. Hanson[4], N. Harty[1], B. Hendricks[11,12], K.D. Hoffman[3], B. Hokanson-Fasig[4], E. Hong[15], S.Y. Hsu[2], J.J. Huang[2], M.-H. Huang [2], K. Hughes[8], A. Ishihara[17], A. Karle[4], J.L. Kelley[4], R. Khandelwal[4], K.-C. Kim[3], M.-C. Kim[4], R. Krebs[11,12], I. Kravchenko[14], Y. Ku[11,12], C.Y. Kuo[2], K. Kurusu[17], U.A. Latif[10,9], A. Laundrie[4], H. Landsman[7], M.-Y. Lu[4], T.-C. Liu [2], B. Madison[10], K. Mase[17], T. Meures[4], J. Nam[2], A. Novikov[10], R.J. Nichol[6], G. Nir[7], A. Nozdrina[10], E. Oberla[8], A. OMurchadha[4], J. Osborn[14], Y. Pan[1], C. Pfendner[5], N. Punsuebsay[1], J. Roth[1], P. Sandstrom[4], D. Seckel[1], Y.-S. Shiao[2], A. Shultz[10], D. Smith[8], J. Torres[15], S. Toscano[18], J. Touart[3], N. van Eijndhoven[9], G.S. Varner[11], A. Vieregg[8], M.-Z. Wang[2], S.-H. Wang[2], Y.H. Wang [2], S.A. Wissel[11,12,20,21], C. Xie[6], R. Young[10], S. Yoshida[17]

[1] Dept. of Physics, University of Delaware, Newark, DE 19716
[2]Dept. of Physics, Grad. Inst. of Astrophys.,Leung Center for Cosmology and Particle Astrophysics, National Taiwan University, Taipei, Taiwan
[3]Dept. of Physics, University of Maryland, College Park, MD 20742
[4]Dept. of Physics, University of Wisconsin-Madison, Madison, WI 53706
[5]Dept. of Physics and Astronomy, Denison University, Granville, Ohio 43023
[6]Dept. of Physics and Astronomy, University College London, London, United Kingdom
[7] Weizmann Institute of Science, Rehovot, Israel
[8]Dept. of Physics, Enrico Fermi Institue, Kavli Institute for Cosmological Physics, University of Chicago, Chicago, IL 60637
[9]Vrije Universiteit Brussel, Brussels, Belgium
[10]Dept. of Physics and Astronomy, University of Kansas, Lawrence, KS 66045
[11]Center for Multi-Messenger Astrophysics, Institute for Gravitation and the Cosmos, Pennsylvania State University, University Park, PA 16802
[12]Dept. of Physics, Pennsylvania State University, University Park, PA 16802
[13]Moscow Engineering Physics Institute, Moscow, Russia
[14]Dept. of Physics and Astronomy, University of Nebraska, Lincoln, Nebraska 68588
[15]Dept. of Physics, Center for Cosmology and AstroParticle Physics, The Ohio State University, Columbus, OH 43210
[16]Dept. of Physics and Astronomy, Michigan State University, East Lansing, Michigan 48824
[17]Dept. of Physics, Chiba University, Chiba, Japan
[18]Université Libre de Bruxelles, Science Faculty CP230, B-1050 Brussels, Belgium
[19]Dept. Physics and Astronomy, Whittier College, Whittier, CA 90602
[20]Dept. of Astronomy and Astrophysics, Pennsylvania State University, University Park, PA 16802
[21]Physics Dept., California Polytechnic State University, San Luis Obispo, CA 93407
[22]Dept. of Physics and Astronomy, University of Hawaii, Manoa, HI 96822

Acknowledgements

We thank the National Science Foundation Office of Polar Programs and Physics Division for their generous support through NSF OPP-902483, Grant NSF OPP-1002483, Grant NSF 1607555, Grant NSF OPP-1359535, Grant NSF OPP-1404212, and Grant NSF OPP-2013134, and Grant NSF 2019597. K. Hughes thanks the NSF for support through DGE-1746045.